



**HAL**  
open science

## The role of oxygen in magnetron-sputtered Ta<sub>3</sub>N<sub>5</sub> thin films for the photoelectrolysis of water

Martin Rudolph, Dana Stanescu, Jose Alvarez, Eddy Foy, Jean-Paul Kleider, H el ene Magnan, Tiberiu Minea, Nathalie Herlin-Boime, Brigitte Bouchet-Fabre, M.C. Hugon

► **To cite this version:**

Martin Rudolph, Dana Stanescu, Jose Alvarez, Eddy Foy, Jean-Paul Kleider, et al.. The role of oxygen in magnetron-sputtered Ta<sub>3</sub>N<sub>5</sub> thin films for the photoelectrolysis of water. *Surface and Coatings Technology*, 2016, 324, pp.620-625. 10.1016/j.surfcoat.2016.09.007 . cea-01478261

**HAL Id: cea-01478261**

**<https://cea.hal.science/cea-01478261>**

Submitted on 11 Mar 2020

**HAL** is a multi-disciplinary open access archive for the deposit and dissemination of scientific research documents, whether they are published or not. The documents may come from teaching and research institutions in France or abroad, or from public or private research centers.

L'archive ouverte pluridisciplinaire **HAL**, est destin ee au d ep ot et  a la diffusion de documents scientifiques de niveau recherche, publi es ou non,  emanant des  tablissements d'enseignement et de recherche fran ais ou  trangers, des laboratoires publics ou priv es.



Contents lists available at ScienceDirect

## Surface &amp; Coatings Technology

journal homepage: [www.elsevier.com/locate/surfcoat](http://www.elsevier.com/locate/surfcoat)

## The role of oxygen in magnetron-sputtered Ta<sub>3</sub>N<sub>5</sub> thin films for the photoelectrolysis of water

M. Rudolph<sup>a,b,\*</sup>, D. Stanescu<sup>c</sup>, J. Alvarez<sup>d</sup>, E. Foy<sup>e</sup>, J.-P. Kleider<sup>d</sup>, H. Magnan<sup>c</sup>, T. Minea<sup>a</sup>, N. Herlin-Boime<sup>b</sup>, B. Bouchet-Fabre<sup>b</sup>, M.-C. Hugon<sup>a</sup>

<sup>a</sup> LPGP, Univ. Paris-Sud/CNRS, Université Paris-Saclay, 91405 Orsay, France

<sup>b</sup> NIMBE, CEA/CNRS, Université Paris-Saclay, 91191 Gif-sur-Yvette, France

<sup>c</sup> SPEC, CEA/CNRS, Université Paris-Saclay, 91191 Gif-sur-Yvette, France

<sup>d</sup> GeePs, CNRS UMR8507, CentraleSupélec, Univ Paris-Sud, Sorbonne Universités-UPMC Univ Paris 06, 91192 Gif-sur-Yvette Cedex, France

<sup>e</sup> LAPA-IRAMAT, NIMBE, CEA, CNRS, Université Paris-Saclay, CEA Saclay, 91191 Gif-sur-Yvette cedex, France

## ARTICLE INFO

## Article history:

Received 31 May 2016

Revised 22 August 2016

Accepted in revised form 2 September 2016

Available online xxx

## Keywords:

Ta<sub>3</sub>N<sub>5</sub>

Tantalum oxynitride

Magnetron sputtering

Photoelectrolysis

## ABSTRACT

Ta<sub>3</sub>N<sub>5</sub> has ideal properties for the efficient water splitting under sunlight illumination, but its formation is only triggered by the incorporation of oxygen in its lattice. As a result, material properties may deviate from those of an ideal Ta<sub>3</sub>N<sub>5</sub> crystal, which can promote or impede the water splitting. This paper is to quantify variations in key properties relevant for the photoelectrolysis as a function of oxygen incorporation and to determine an optimum oxygen concentration. Thin films were prepared by direct current magnetron sputtering in an Ar/N<sub>2</sub>/O<sub>2</sub> gas mixture at two different N<sub>2</sub> and varying O<sub>2</sub> concentrations. The films were characterized by grazing-incidence x-ray diffraction (GI-XRD), total transmission and reflectance spectroscopy (TTRS) from which the band gap is deduced, photocurrent measurements on which the calculation of the efficiency-mobility-lifetime ( $\eta_{\mu\tau}$ ) product is based and photoelectrolysis experiments. Finally, the stability of films was determined by x-ray photoelectron spectroscopy (XPS) measured before and after the photoelectrolysis. We show that material properties degrade with oxygen incorporation during the film growth. At the highest oxygen concentrations investigated, the material becomes amorphous and shows strong surface oxidation and a possible reaction with the electrolyte during the photoelectrolysis. Samples deposited at an oxygen concentration below 1%, exhibit the Ta<sub>3</sub>N<sub>5</sub> phase, a band gap below 2.0 eV, a high mobility-lifetime product, photoelectrolytic activity and a good relative stability against surface oxidation during the photoelectrolysis.

© 2016 Elsevier B.V. All rights reserved.

### 1. Introduction

Ta<sub>3</sub>N<sub>5</sub> is an ideal candidate for the efficient photoelectrolysis of water under sunlight illumination thanks to its peculiar electronic band structure with a conduction band minimum below the hydrogen evolution potential and a valence band above the oxygen evolution potential [1]. In addition, it absorbs a large portion of the solar spectrum due to its small band gap of 2.1 eV which is close to the optimum band gap for solar water splitting (around 2.0 eV [2]).

A common synthesis method of crystalline Ta<sub>3</sub>N<sub>5</sub> is the ammonolysis or nitridation of a Ta<sub>2</sub>O<sub>5</sub> foil, but also radio-frequency magnetron sputtering in an Ar/N<sub>2</sub>/O<sub>2</sub> gas [3]. All synthesis methods have in common that oxygen plays a crucial role in triggering the crystallization process. This is due to the inductive effect in which the stability of a compound with a high oxidation state transition metal is increased by

replacing its bonding partner with an atom having a higher electronegativity [4]. In the case of Ta<sub>3</sub>N<sub>5</sub>, the partial replacement of nitrogen with oxygen stabilizes the compound with a Ta atom in a +5 oxidation state.

The incorporation of oxygen changes the properties of the Ta<sub>3</sub>N<sub>5</sub>-crystallized material which raises the question whether these modifications are beneficial for the use of the material as a photoanode for solar water splitting. Recent calculations have shown that a positive effect is expected at least for the onset potential in the photoelectrolysis [5]. Experimental evidence for the changes of key material properties with oxygen incorporation, on the other hand, are rare in the literature.

We employed direct current (DC) magnetron sputtering to prepare films of Ta(-O)-N with varying oxygen concentration to follow the evolution of material properties relevant to the photoelectrolysis: crystalline structure, band gap and the efficiency-mobility-lifetime product. The chemical stability of the films was evaluated by x-ray photoelectron spectroscopy that was conducted on the same samples before and after photoelectrolysis. These measurements provide a comprehensive picture of the influence of oxygen on magnetron-sputtered Ta<sub>3</sub>N<sub>5</sub> thin films.

\* Corresponding author at: LPGP, Univ. Paris-Sud/CNRS, Université Paris-Saclay, 91405 Orsay, France.

E-mail address: [martin.rudolph@u-psud.fr](mailto:martin.rudolph@u-psud.fr) (M. Rudolph).

## 2. Thin film preparation

Thin films were deposited in a direct current magnetron discharge using a balanced magnetron with a Ta target of 99.95% purity that was 10 cm in diameter. As a substrate, we chose a conductive Ta foil and an insulating, transparent piece of quartz to comply with different measurement techniques. Each sample was deposited onto both substrates simultaneously.

Before deposition, the substrates were cleaned in isopropyl alcohol and then placed under vacuum for radio-frequency sputtering for 10 min at an effective DC bias of 100 V. The vacuum remained unbroken between cleaning and deposition. At the same time, the target was cleaned with a closed shutter for 20 min in pure Ar at 0.5 Pa, then for further 10 min in the gas mixture in which the sample was deposited after cleaning.

All samples were deposited at a pressure of 0.5 Pa on a substrate maintained at a temperature around 870 K measured by a thermocouple inside the heating ceramics on which the substrates were clamped. The injected N<sub>2</sub> gas had a concentration c<sub>N<sub>2</sub></sub> of 40% and 60% and the oxygen concentration was varied between 0.4% and 2.6%. Argon was added to reach a total flow rate of 50 sccm for c<sub>N<sub>2</sub></sub> = 40% and a flow rate of 25 sccm for c<sub>N<sub>2</sub></sub> = 60%. The different total flow rates were necessary for technical reasons. It should be kept in mind that the same c<sub>O<sub>2</sub></sub> has half the O<sub>2</sub> flow rate at a total flow rate of 50 sccm compared to a total flow rate of 25 sccm. As films deposited at c<sub>N<sub>2</sub></sub> = 60% were also around 40% thinner (see below), the parameter “concentration” correlates approximately with the amount of oxygen incorporated into the films. This can be seen below as all plots as a function of c<sub>O<sub>2</sub></sub> show that data points for c<sub>N<sub>2</sub></sub> = 40% and c<sub>N<sub>2</sub></sub> = 60% lie roughly on one line. Throughout this paper, the term concentration will be used to denote the volumetric concentration in percent in the working gas mixture injected into the reactor.

The inspection of the plasma discharge by optical emission spectroscopy did not reveal any oxygen lines at low concentrations and only a small signal at the higher concentrations. This indicates that the target remains in the metallic mode with respect to the oxygen, i.e. injected oxygen is immediately gettered by the deposited Ta and by the target [6]. As a consequence, we expect an incorporation of oxygen into the film that is linear with the oxygen concentration in the injected gas mixture.

All samples were deposited for 30 min which resulted in thicknesses of 330 nm to 380 nm at c<sub>N<sub>2</sub></sub> = 40% and 200 to 250 nm at c<sub>N<sub>2</sub></sub> = 60% as determined from the fitted UV/VIS spectra. The films were stored under N<sub>2</sub> for the short time between the deposition and the measurements.

## 3. Thin film characterization

### 3.1. Characterization methods

#### 3.1.1. Grazing-incidence x-ray diffraction (GI-XRD)

GI-XRD was performed at an angle of 0.5° with respect to the sample surface using the K<sub>α</sub> line of Mo at λ = 0.070932 nm. The sample was moved into the incident plane of a beam of 30 μm in diameter by detecting the maximum fluorescent signal of the tantalum L-edge. An x-ray sensitive image plate behind the sample recorded all diffraction angles simultaneously up to a wave vector of  $q = 4\pi/\lambda \sin(0.5 \cdot 2\theta) = 30 \text{ nm}^{-1}$  which resulted in typical circular diffraction patterns. These were then angularly integrated to yield the diffractograms. All diffractograms presented here show the raw data without any background subtraction.

#### 3.1.2. Total transmission and reflectance spectroscopy (TTRS)

The total transmission and reflection spectroscopy (TTRS) of samples deposited on quartz were determined using a photospectrometer. The samples were clamped onto the port of an integrating sphere

which collected the transmitted or reflected intensity respectively which was then put into relation with the 100% baseline signal to obtain the transmission and reflection value as a function of the wavelength. The monochromator slit width was 2 nm and the wavelengths ranged from 350 to 1000 nm.

The transmission and reflection signal were subsequently fitted to a Tauc-Lorentz model with a single oscillator [7]. In some cases this model was extended by an Urbach tail [8]. These models parameterize the complex relative permittivity  $\epsilon_r = \epsilon_1 + i\epsilon_2$  and use the band gap and the film thickness, among others, as parameters which are thus directly accessible through the model. The absorption coefficient  $\alpha = 4\pi k/\lambda$ , used to calculate the efficiency-mobility-lifetime product ( $\eta\mu\tau$ ), with  $k = 0.5[(\epsilon_1^2 + \epsilon_2^2)^{1/2} - \epsilon_1]^{1/2}$ , is calculated directly from the relative permittivity. The fitting was automated using an in-house code based on a global optimization algorithm [9].

#### 3.1.3. X-ray photoelectron spectroscopy (XPS)

X-ray photoelectron spectroscopy (XPS) was used to reveal the chemical bonding of the Ta atoms inside the film. The spectra were calibrated in energy by shifting the 4f<sub>7/2</sub> peak of a gold sample to a binding energy of 84 eV. Measurements were then done using the samples deposited on a Ta foil which were stuck onto a quartz slide to achieve the same electrical insulation for all samples. The charging of the samples by ejected electrons was compensated by an electron gun. The compensation was verified by assuring that the Au peak did not move for each batch of samples.

#### 3.1.4. Conductivity and efficiency-mobility-lifetime ( $\eta\mu\tau$ ) product

The electronic transport properties were investigated by depositing two coplanar electrodes of silver on the sample surfaces. For this, the same samples as for the TTRS measurements, namely those deposited on insulating quartz substrates, were used.

Current–Voltage (I–V) measurements were performed in both dark condition and under illumination. The illumination system consisted of a calibrated blue LED light source emitting at 450 nm. The integrated photon flux used for the photocurrent measurements was evaluated to 10<sup>15</sup> photons · cm<sup>-2</sup> · s<sup>-1</sup>. The I–V curves (not illustrated here) showed an ohmic behavior under dark and illumination for the voltage range between –5 V and +5 V. The determination of the efficiency-mobility-lifetime ( $\eta\mu\tau$ ) product relied on measuring the photoconductivity of Ta<sub>3</sub>N<sub>5</sub> films under above band-gap steady-state illumination. This notably implied to know the film thickness, the optical absorption and surface reflectivity at 450 nm, the applied voltage and the electrode geometry. The details of the calculation of the  $\eta\mu\tau$  product can be found in [10].

#### 3.1.5. Photoelectrolysis

The photoelectrochemical properties of the samples were studied using a three-electrode photoelectrochemical cell described in detail in [11] except that we used a different electrolyte (0.1 M K<sub>2</sub>SO<sub>4</sub> adjusted with KOH to reach pH = 11, similar to [12]). The samples were illuminated by a Xe arc lamp at a power density of 100 mW/cm<sup>2</sup>. Each sample was subjected to voltammetry between –0.5 and 0.6 V vs. Ag/AgCl under chopped white light illumination. After the measurement, the samples were rinsed with distilled water and in this way prepared for a second XPS measurement.

## 3.2. Characterization results

### 3.2.1. Grazing-incidence X-ray diffraction (GI-XRD)

The presence of the Ta<sub>3</sub>N<sub>5</sub> phase is evidenced by GI-XRD (Fig. 1). For both nitrogen concentrations tested (40% and 60%), the Ta<sub>3</sub>N<sub>5</sub> phase appears for samples at intermediate c<sub>O<sub>2</sub></sub> and is observed for a certain range of oxygen concentrations. At the upper limit of oxygen concentrations investigated, i.e. for c<sub>O<sub>2</sub></sub> = 1.8% the diffractograms become featureless,

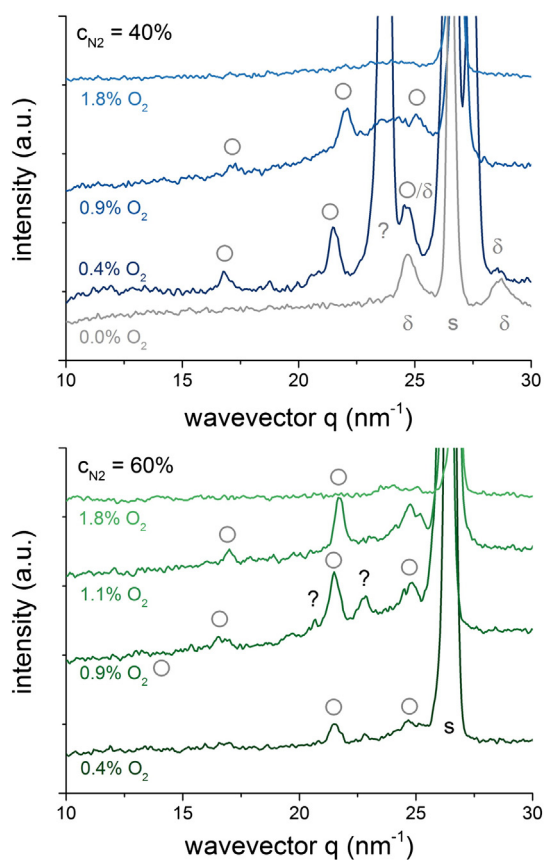


**Fig. 1.** Diffractograms for  $c_{N_2} = 40\%$  (top) and  $60\%$  (bottom) at varying oxygen concentrations  $c_{O_2}$ . The peaks corresponding to  $Ta_3N_5$  (orthorhombic, Powder diffraction file (PDF) 01-079-1533) are marked by 'o', peaks corresponding to  $\delta$ -TaN (NaCl-type, PDF 01-089-5197) are marked by 'δ', peaks that could not be unambiguously attributed are marked by '?' and the peak corresponding to the underlying Ta substrate (Ta, body-centered cubic, PDF 01-089-5196) is marked by 's'.

indicating an amorphous phase. At very low oxygen concentrations, we observe a transition to the metallic  $\delta$ -TaN phase. At  $c_{O_2} = 0.4\%$ , peaks of the metallic phase appear that are still weak in intensity, but become dominant for the sample at  $c_{O_2} = 0.0\%$ . Thus, under our experimental conditions, it is necessary to incorporate oxygen into the lattice to stabilize the  $Ta_3N_5$  phase, the reason for which was discussed in the introduction.

### 3.2.2. Band gap measurements

The band gap for each sample is determined from the simultaneous inversion of the total transmission and reflectance spectra (TTRS). The samples at high oxygen concentration are fitted using a single oscillator Tauc-Lorentz (TL) model [7]. This model can be applied for samples with an oxygen concentration ( $c_{O_2}$ ) higher than 1.0% for both  $c_{N_2}$ . For sample with oxygen concentrations less than 1.0%, the transmission below the band gap energy, i.e. in the long wavelength range, diminishes, which indicates the presence of in-gap states that cannot be represented by a simple Tauc-Lorentz model any more. Therefore, an Urbach tail (UT) model is added to the single oscillator TL model which results in good fits (Fig. 2). An explanation for these states could be the onset of metallic bond formation as these states appear in the transition region between the pure  $Ta_3N_5$  and the metallic  $\delta$ -TaN phase as observed by GI-XRD.

The band gap of all samples follows approximately the same trend line irrespective of the model used for fitting. It widens with  $c_{O_2}$  (Fig. 3) which is a direct effect of the increased incorporation of oxygen into the lattice [13] [14]. Samples deposited at a low  $c_{O_2}$  have a band gap of 1.3 eV, samples at the highest  $c_{O_2}$  show a band gap of 2.6 eV.

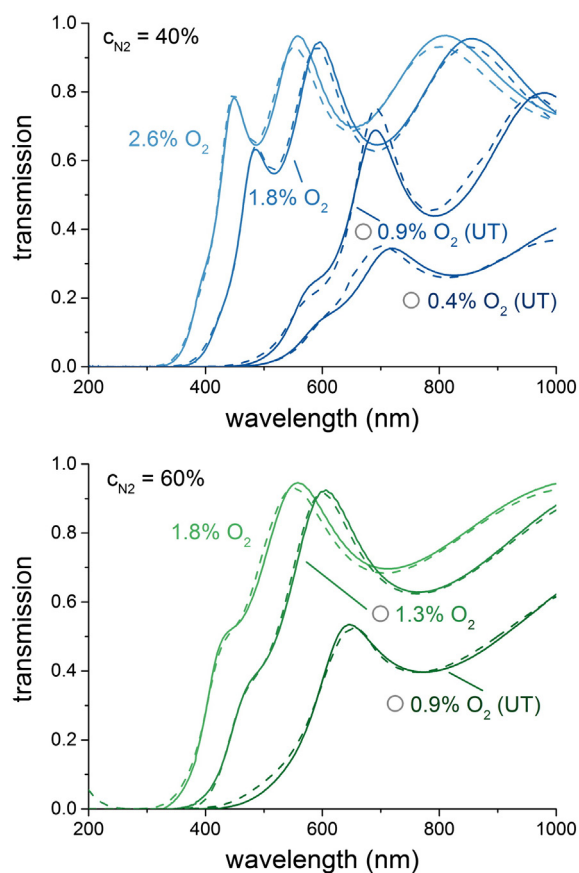


**Fig. 2.** UV/VIS transmission spectra of experimental (continuous line) and fitted (dashed line) for  $c_{N_2} = 40\%$  (top) and  $60\%$  (bottom). The sample at  $c_{N_2} = 40\%$  and  $c_{O_2} = 0.0\%$  showed no transmission for any wavelengths as expected for a metallic sample and is therefore not plotted. The curves fitted with the Tauc-Lorentz model complemented by an Urbach tail model are marked by (UT). The reflection spectra are omitted but were used simultaneously with the transmission spectra in the fitting procedure. Grey circles indicate samples with the  $Ta_3N_5$  phase.

The samples at high  $c_{O_2}$  are already amorphous, though, so that the range of band gaps should be limited to the last sample showing the crystalline  $Ta_3N_5$  phase, which is the sample at  $c_{O_2} = 1.3\%$  ( $c_{N_2} = 60\%$ ) having a band gap of 2.0 eV. These values are low compared to

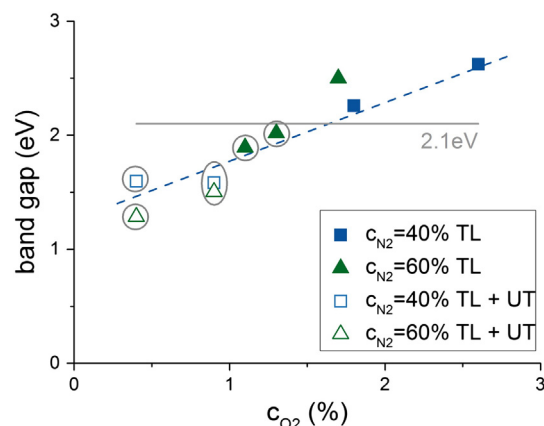


**Fig. 3.** Band gap retrieved from fitting the total transmission and reflectance spectra to a single oscillator Tauc-Lorentz (TL) model (solid squares) or to a TL model complemented by an Urbach tail (TL + UT, open squares) for  $c_{N_2} = 40\%$  (blue) and  $60\%$  (green). A trend line is shown for samples deposited at  $c_{N_2} = 40\%$ . Grey circles indicate samples with the  $Ta_3N_5$  phase. (For interpretation of the references to colour in this figure legend, the reader is referred to the web version of this article.)

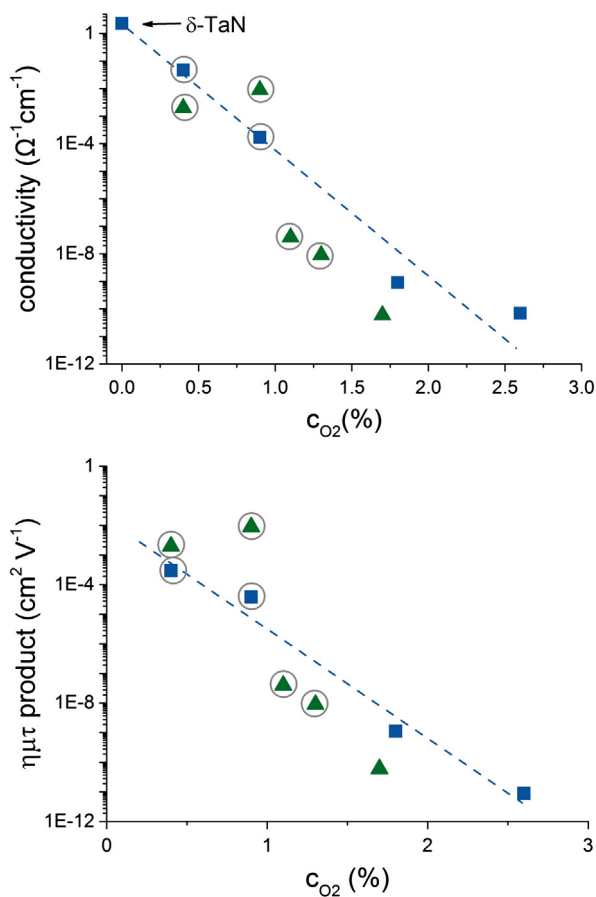


**Fig. 4.** Conductivity (top) and efficiency-mobility-lifetime ( $\eta\mu\tau$ ) product (bottom). A trend line is shown for  $c_{N_2} = 40\%$  in each of the plots. Grey circles indicate samples with the  $Ta_3N_5$  phase.

experimentally determined band gaps in literature for  $Ta_3N_5$  films prepared by ammonolysis of  $Ta_2O_5$ , that have band gaps of  $\sim 2.0$  eV [15] and 2.1 eV [13]. This could, again, be rationalized by the in-gap states, that successively narrow the band gap. However, already the samples without observable in-gap states at  $c_{O_2} = 1.1\%$  and  $1.3\%$  ( $c_{N_2} = 60\%$ ) have band gaps of 1.9 eV and 2.0 eV which are lower than those measured for films deposited by ammonolysis. Responsible for this could be less oxygen in our samples. But as neither for the films prepared by ammonolysis nor for our films, the absolute oxygen content was determined, this remains a hypothesis. It is known however that even the ammonolysis of  $Ta_2O_5$  leaves some oxygen in the film [16].

**3.2.3. Conductivity and efficiency-mobility-lifetime ( $\eta\mu\tau$ ) product**

The conductivity of all samples is presented in Fig. 4 (top). A trend line for the samples deposited at  $c_{N_2} = 40\%$  indicates a linear evolution of the conductivity with  $c_{O_2}$ . This linear trend extends even up to the sample showing the metallic  $\delta$ -TaN phase at  $c_{O_2} = 0.0\%$ , which supports our argument from above that less incorporated oxygen renders a sample increasingly metallic. The plot shows in addition that this transition from a semiconducting phase to a metallic phase is smooth.

The  $\eta\mu\tau$  product describes the average distance charge carriers diffuse before recombining. Its evolution as a function of  $c_{O_2}$  follows the same trend as the conductivity. It exhibits a very low value for the films deposited at a high oxygen concentration. The amorphous structure found for those films can be held responsible for this as a reduced crystallinity typically promotes recombination. Another type of recombination center may be introduced by the oxygen in the lattice, that is known to form deep-level defects as evidenced by photoluminescence experiments [17]. Towards the lowest  $c_{O_2}$ , the  $\eta\mu\tau$  product increases

over nine orders of magnitude indicating a much improved charge carrier diffusion length.

A reference value for the mobility-lifetime product was published in [18] for films of  $Ta_3N_5$ . They were prepared by sputtering films of Ta-N in an Ar/ $N_2$  gas mixture at room temperature followed by annealing in air and in  $NH_3$ . The authors determined a  $\mu\tau$  product around  $10^{-11} cm^2 V^{-1} s^{-1}$ , which is low compared to our measurements and which we only find for amorphous films at the highest oxygen concentrations. Similar to the difference in band gaps between our magnetron-sputtered films and those prepared by ammonolysis, the difference in the  $\mu\tau$  product could be ascribed to an unequal amount of remaining oxygen in the films of both studies. This is in line with our findings, as a reduced oxygen concentration increases the  $\eta\mu\tau$ . Consequently, as little

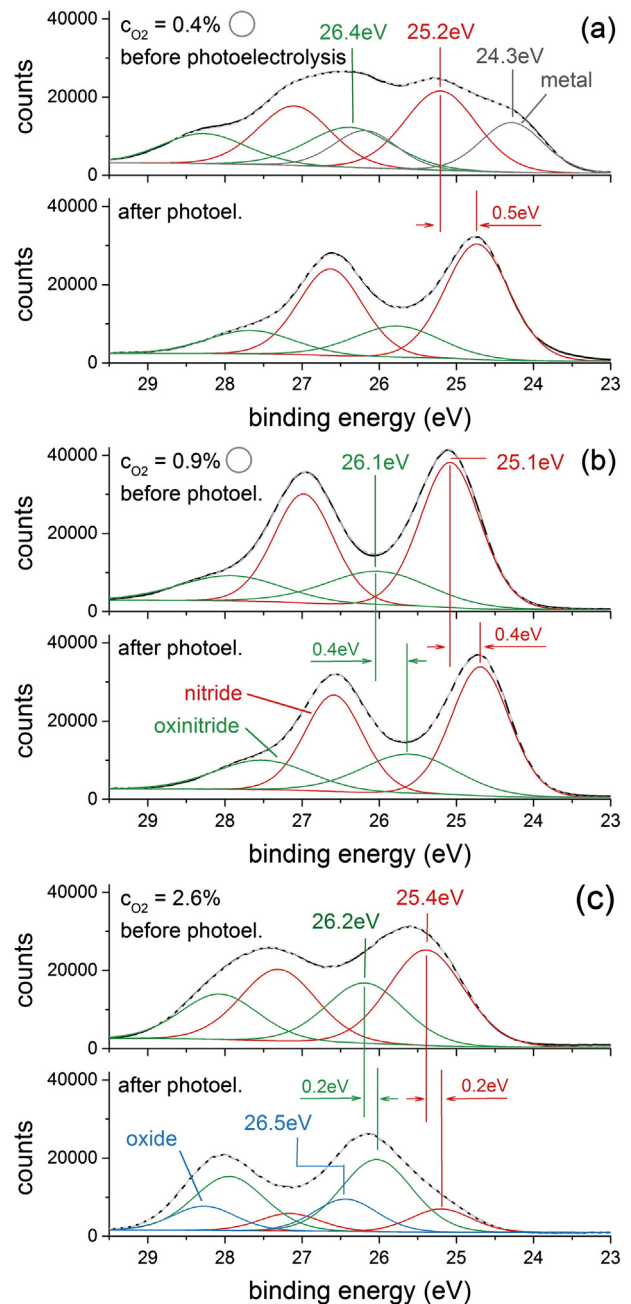


**Fig. 5.** Evolution of the XPS spectra of the Ta 4f region for samples deposited at  $c_{N_2} = 40\%$  as a function of oxygen concentration,  $c_{O_2} = 0.4\%$  (a),  $c_{O_2} = 0.9\%$  (b) and  $c_{O_2} = 2.4\%$  (c), measured before (top) and after (bottom) the photoelectrolysis. Grey circles indicate samples with the  $Ta_3N_5$  phase.

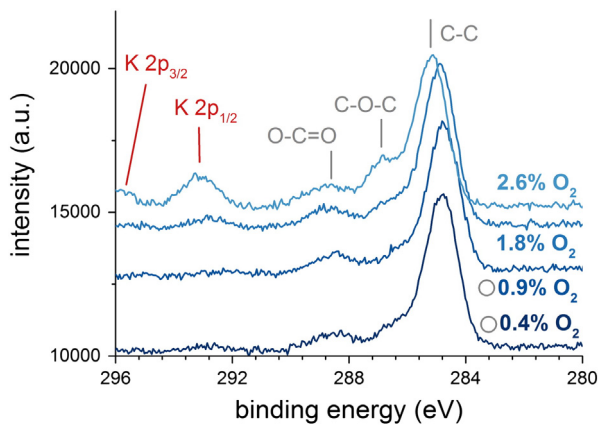


**Fig. 6.** Carbon 1s spectra of the samples deposited at  $c_{N_2} = 40\%$  after photoelectrolysis measured by x-ray photoelectron spectroscopy. Potassium peaks for the two samples at  $c_{O_2} = 1.8\%$  and  $c_{O_2} = 2.6\%$  hint towards a surface reaction with the electrolyte. Grey circles indicate samples with the  $Ta_3N_5$  phase.

oxygen as possible should be incorporated into  $Ta_3N_5$  thin films for a high charge carrier diffusion length.

3.2.4. X-ray photoelectron spectroscopy (XPS)

XPS was used to study the stability of the film during photoelectrolysis. As the 40% and 60% nitrogen concentrations gave similar trends, only the samples deposited at  $c_{N_2} = 40\%$  are discussed in the following.

The samples measured before and after the photoelectrolysis are presented in Fig. 5. Before photoelectrolysis, all spectra are fitted using a minimum of two doublets. The one at lower binding energies, we name nitride, as their Ta  $4f_{7/2}$  binding energy peaks between 25.1 eV and 25.4 eV lie close to the  $Ta_3N_5$  peak at 24.8 eV [1]. The one at high binding energies, we name oxynitride, as their Ta  $4f_{7/2}$  binding energy peaks between 26.1 eV and 26.4 eV lie close to the TaON peak at 25.8 eV [1]. The first sample at  $c_{O_2} = 0.4\%$  has an additional doublet at even lower energy which is named metal doublet due to its proximity to the Ta  $4f_{7/2}$  peak in TaN at 23.5 eV [19]. All of these peaks are slightly shifted to higher binding energies by 0.2 to 0.8 eV compared to their reference values.

After the photoelectrolysis, i.e. having placed the samples in a basic solution for about 30 min during which the photoelectrolysis measurement took place (see paragraph 5), the nitride and oxynitride doublets are still present in all samples. They are slightly shifted compared to their initial positions by 0.2 to 0.5 eV to lower binding energies. However, as oxygen is evolved on the sample surface during the photoelectrolysis, it is unlikely that the semiconductor surface is reduced in this environment.

A striking change induced by the photoelectrolysis is the number of doublets necessary to obtain a good fit. On the sample deposited at lowest  $c_{O_2}$ , the metallic doublet disappears and the sample deposited at highest  $c_{O_2}$  gains an additional doublet. This latter doublet has a Ta

**Table 1**

Area ratios of nitride component to oxynitride and, if present, oxide component,  $r = \frac{S_N}{S_{ON} + S_O}$  before and after the photoelectrolysis. Grey circles indicate samples with the  $Ta_3N_5$  phase.

$c_{N_2}, c_{O_2}$	$r_{before}$	$r_{after}$	$(r_{before} - r_{after}) / r_{before} (\%)$
40%, 0.9% ○	2.6	2.1	-19%
40%, 1.8% ○	1.6	0.8	-46%
40%, 2.6% ○	1.5	0.7	-55%
60%, 0.9% ○	2.0	1.9	-5%
60%, 1.3% ○	2.6	0.5	-79%
60%, 1.7% ○	2.1	0.4	-82%

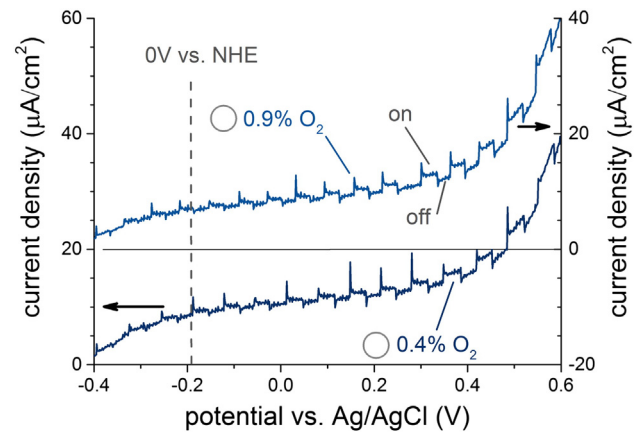


**Fig. 7.** On-off photocurrent curves for two  $Ta_3N_5$ -crystalline samples deposited a  $c_{N_2} = 40\%$ . Both samples show the  $Ta_3N_5$  phase.

$4f_{7/2}$  binding energy peak at 26.5 eV and is very close to the  $Ta_2O_5$  reference value at 26.6 eV [1] which reveals surface oxidation of the sample by the photoelectrolysis. Further evidence for the non-stability of the film surface at highest  $c_{O_2}$  can be seen on the carbon 1s spectra (Fig. 6) which shows the appearance of a potassium peak after photoelectrolysis and hints towards a reaction between the semiconductor and the electrolyte.

Additional insight can be gained by looking at the peak areas of the fitted components. We calculate the area ratios of the nitride  $S_N$  to the oxynitride  $S_{ON}$  and, if present, oxide component  $S_O$ ,  $r = \frac{S_N}{S_{ON} + S_O}$  and exclude the sample with a metallic component. For all six samples, the nitride-to-oxide area ratios decrease between before and after photoelectrolysis. This is in line with other authors that have observed a surface oxidation of  $Ta_3N_5$  in water [3] [20] similar to our findings. This altered surface reduces the photocurrent [21], but it does not necessarily inhibit the functioning of the device even in the long term, as the oxidized surface serves as a protection layer and inhibits further oxidation of the bulk [20].

Complementary to other studies, we find a correlation between the extent of surface oxidation and the amount of oxygen in the films as the films deposited at low  $c_{O_2}$ , are much less prone to surface oxidation (Table 1), showing that films with little incorporated oxygen have an improved stability of their surface under photoelectrolysis conditions.

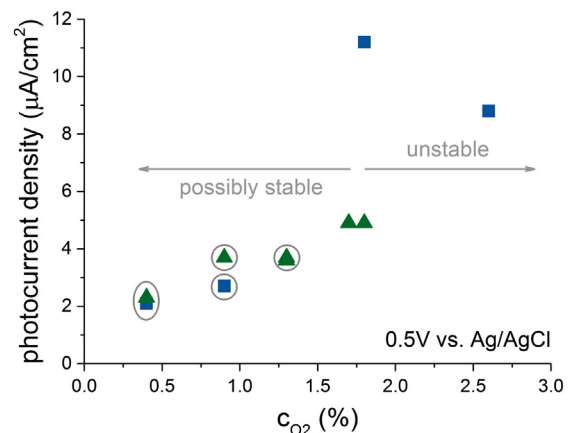


**Fig. 8.** Photocurrent of all samples at 0.5 V vs. the silver chloride electrode (Ag/AgCl) for samples deposited at  $c_{N_2} = 40\%$  (blue) and  $c_{N_2} = 60\%$  (green) as a function of  $c_{O_2}$ . Grey circles indicate samples with the  $Ta_3N_5$  phase. (For interpretation of colour in this figure legend, the reader is referred to the web version of this article.)

#### 4. Photoelectrolysis

Finally, we studied the photoelectrochemical properties of the samples. Fig. 7 shows current density curves as a function of the applied potential for two samples deposited at low oxygen concentration. The samples were measured under chopped light illumination which results in the fragmented curve with an upper plateau corresponding to the current during illumination and the lower plateau to the dark current. The difference between these two curves is the photocurrent. High transients can be observed at the beginning and at the end of each illumination pulse which are typically attributed to the low rate constant for water oxidation [22].

The onset potential, i.e. the minimum potential at which an effect of the light is observed, is small, which is beneficial for efficient solar water splitting. Already around 0 V vs. the normal hydrogen electrode (NHE) a small photocurrent evolves which proves that bias-free photoelectrolysis of water by Ta<sub>3</sub>N<sub>5</sub> is possible.

A summary of the photocurrent densities for all samples measured at a bias of 0.5 V vs. the silver chloride electrode (Ag/AgCl) is given in Fig. 8. We observe two groups of samples that can be distinguished by their photocurrent densities. One group, deposited at high c<sub>O<sub>2</sub></sub>, contains only two samples that show a comparably high photocurrent density between 8 μA/cm<sup>2</sup> and 12 μA/cm<sup>2</sup>. These two samples are those reacting with the electrolyte as evidenced by the XPS measurements (Fig. 6). The high photocurrent may thus be an effect of this reaction and we conclude that the samples deposited at high c<sub>O<sub>2</sub></sub> are not stable under our photoelectrolysis conditions.

A second group of samples shows a low photocurrent between 2 and 5 μA/cm<sup>2</sup>. Among those, a direct comparison between samples is difficult due to the difference in their thicknesses. However, the measured photocurrent is small on all those samples compared to other magnetron-sputtered Ta<sub>3</sub>N<sub>5</sub> films [3] where the samples were annealed in NH<sub>3</sub> which increases the crystallinity and the photocurrent [3]. Moreover, we did not vary the thickness of the films which is certainly an important parameter to find a good compromise between photon absorption and charge carrier recombination [11].

#### 5. Conclusion

We investigated the variation of material properties of Ta<sub>3</sub>N<sub>5</sub> thin films as a function of oxygen concentration in the injected gas mixture and evaluated its use as a photoanode for solar water splitting.

A clear degradation of properties of the Ta<sub>3</sub>N<sub>5</sub> crystalline phase with incorporation of oxygen is evidenced. The efficiency-mobility-lifetime product decreases over ten orders of magnitude within the small range of oxygen concentrations, the band gap widens and the stability in photoelectrolysis is drastically reduced.

Oxygen, although necessary to trigger the crystallization of the Ta<sub>3</sub>N<sub>5</sub> phase, should be kept to a minimum in magnetron-sputtered films. For the deposition reactor configuration and the magnetron used in this study, an oxygen concentration between 0.4 and 0.9% was found to be the optimum value and we show in this case that Ta<sub>3</sub>N<sub>5</sub> can be used as a photoanode for solar water splitting.

#### Acknowledgements

The authors are grateful for the funding of this activity by the Centre National de la Recherche Scientifique (CNRS) under the grant

agreement ANR-13-IS09-0003-01. We would also like to thank Martine Wery for an insightful discussion on electrochemistry and Jocelyne Leroy and Séverine Le Moal for sharing their knowledge on XPS measurements and fittings.

#### References

- [1] W.-J. Chun, A. Ishikawa, H. Fujisawa, T. Takata, J.N. Kondo, H. Michikazu, M. Kawai, Y. Matsumoto, K. Domen, Conduction and valence band positions of Ta<sub>2</sub>O<sub>5</sub>, TaON, and Ta<sub>3</sub>N<sub>5</sub> by UPS and electrochemical methods, *J. Phys. Chem. B* 107 (2003) 1798–1803.
- [2] A.B. Murphy, P.R.F. Barnes, L.K. Randeniya, I.C. Plumb, I.E. Grey, M.D. Horne, J.A. Glasscock, Efficiency of solar water splitting using semiconductor electrodes, *Int. J. Hydrog. Energy* 31 (2006) 1999–2017.
- [3] D. Yokoyama, H. Hashiguchi, K. Maeda, T. Minegishi, T. Takata, R. Abe, J. Kubota, K. Domen, Ta<sub>3</sub>N<sub>5</sub> photoanodes for water splitting prepared by sputtering, *Thin Solid Films* 519 (2011) 2087–2092.
- [4] J. Etourneau, J. Portier, F. Ménéil, The role of the inductive effect in solid state chemistry: how the chemist can use it to modify both the structural and the physical properties of the materials, *J. Alloys Compd.* 188 (1992) 1–7.
- [5] M. Harb, P. Sautet, E. Nurlaela, P. Raybaud, L. Cavallo, K. Domen, J.-M. Basset, K. Takanabe, Tuning the properties of visible-light-responsive tantalum (oxy)nitride photocatalysts by non-stoichiometric compositions: a first-principles viewpoint, *Phys. Chem. Chem. Phys.* 16 (2014) 20548–20560.
- [6] G.S. Chen, C.C. Lee, H. Niu, W. Huang, R. Jann, T. Schütte, Sputter deposition of titanium monoxide and dioxide thin films with controlled properties using optical emission spectroscopy, *Thin Solid Films* 516 (2008) 7473–7478.
- [7] G.E. Jellison, J. Modin, F.A. Modine, Parameterization of the optical functions of amorphous materials in the interband region, *Appl. Phys. Lett.* 69 (3) (1996) 371–373.
- [8] A.S. Ferlauto, G.M. Ferreira, J.M. Pearce, C.R. Wronski, R.W. Collins, X. Deng, G. Ganguly, Analytical model for the optical functions of amorphous semiconductors from the near-infrared to ultraviolet: applications in thin film photovoltaics, *J. Appl. Phys.* 92 (5) (2002) 2424–2436.
- [9] T. Csendes, L. Pál, J.O.H. Sendin, J.R. Banga, The GLOBAL optimization method revisited, *Optim. Lett.* 2 (2008) 445–454.
- [10] W. Jackson, N.M. Amer, R.J. Nemanich, Energy dependence of the carrier mobility-lifetime product in hydrogenated amorphous silicon, *Phys. Rev. B* 27 (8) (1983) 4861–4871.
- [11] M. Rioult, H. Magnan, D. Stanesco, A. Barbier, Single crystalline hematite films for solar water splitting: Ti-doping and thickness effects, *J. Phys. Chem. C* 118 (6) (2014) 3007–3014.
- [12] A. Ishikawa, T. Takata, J. Kondo, M. Hara, K. Domen, Electrochemical behavior of thin Ta<sub>3</sub>N<sub>5</sub> semiconductor film, *J. Phys. Chem. B* 108 (2004) 11049–11053.
- [13] K. Maeda, K. Domen, New non-oxide photocatalysts designed for overall water splitting under visible light, *J. Phys. Chem. C* 111 (2007) 7851–7861.
- [14] V. Tiron, V. Sirghi, Tuning the band gap and nitrogen content of ZnOxNy thin films deposited by reactive HiPIMS, *Surf. Coat. Technol.* 282 (2015) 103–106.
- [15] J.M. Morbec, I. Narkeviciute, T.F. Jaramillo, G. G., Optoelectronic properties of Ta<sub>3</sub>N<sub>5</sub>: a joint theoretical and experimental study, *Phys. Rev. B* 9 (2014) 155204.
- [16] S.J. Henderson, A.L. Hector, Structural and compositional variations in Ta<sub>3</sub>N<sub>5</sub> produced by high-temperature ammonolysis of tantalum oxide, *J. Solid State Chem.* 179 (11) (2006) 3518–3524.
- [17] G. Fu, S. Yan, T. Yu, Z. Zou, Oxygen related recombination defects in Ta<sub>3</sub>N<sub>5</sub> water splitting photoanode, *Appl. Phys. Lett.* 107 (2015) 171902.
- [18] A. Ziani, E. Nurlaela, D.S. Dhawale, D.A. Silva, E. Alarousu, O.F. Mohammed, K. Takanabe, Carrier dynamics of a visible-light-responsive Ta<sub>3</sub>N<sub>5</sub> photoanode for water oxidation, *Phys. Chem. Chem. Phys.* 17 (2015) 2670–2677.
- [19] Q.Y. Zhang, X.X. Mei, D.Z. Yang, F.X. Chen, T.C. Ma, Y.M. Wang, F.N. Teng, Preparation, structure and properties of TaN and TaC films obtained by ion beam assisted deposition, *Nucl. Instr. Meth. Phys. Res.* 127–128 (1997) 664–668.
- [20] M. Hara, E. Chiba, A. Ishikawa, T. Takata, J.N. Kondo, K. Domen, Ta<sub>3</sub>N<sub>5</sub> and TaON thin films on Ta foil: surface composition and stability, *J. Phys. Chem. B* 107 (2003) 13441–13445.
- [21] M. Li, W. Luo, D. Cao, X. Zhao, Z. Li, T. Yu, Z. Zou, A co-catalyst-loaded Ta<sub>3</sub>N<sub>5</sub> photoanode with a high solar photocurrent for water splitting upon facile removal of the surface layer, *Angew. Chem. Int. Ed. Eng.* 52 (42) (2013) 11016–11020.
- [22] H. Dotan, K. Sivula, M. Grätzel, A. Rothschild, S.C. Warren, Probing the photoelectrochemical properties of hematite (α-Fe<sub>2</sub>O<sub>3</sub>) electrode using hydrogen peroxide as a hole scavenger, *Energy Environ. Sci.* 4 (2011) 958–964.